

Phase separation of binary mixtures in thin films: Effects of an initial concentration gradient across the film

Prabhat K. Jaiswal,^{1,2} Kurt Binder,¹ and Sanjay Puri²¹*Institut für Physik, Johannes Gutenberg-Universität Mainz, Staudinger Weg 7, D-55099 Mainz, Germany*²*School of Physical Sciences, Jawaharlal Nehru University, New Delhi 110067, India*

(Received 24 October 2011; revised manuscript received 20 January 2012; published 13 April 2012)

We study the kinetics of phase separation of a binary (A,B) mixture confined in a thin film of thickness D by numerical simulations of the corresponding Cahn-Hilliard-Cook (CHC) model. The initial state consisted of 50% A:50% B with a concentration gradient across the film, i.e., the average order parameter profile is $\Psi_{av}(z, t = 0) = (2z/D - 1)\Psi_g$, $0 \leq z \leq D$, for various choices of Ψ_g and D . The equilibrium state (for time $t \rightarrow \infty$) consists of coexisting A-rich and B-rich domains separated by interfaces oriented perpendicular to the surfaces. However, for sufficiently large Ψ_g , a (metastable) layered state is formed with a single interface parallel to the surfaces. This phenomenon is explained in terms of a competition between domain growth in the bulk and *surface-directed spinodal decomposition* (SDSD) that is caused by the gradient. Thus, gradients in the initial state can stabilize thin-film morphologies which are not stable in full equilibrium. This offers interesting possibilities as a method for preparing novel materials.

DOI: [10.1103/PhysRevE.85.041602](https://doi.org/10.1103/PhysRevE.85.041602)

PACS number(s): 68.15.+e, 64.75.Nx, 64.75.Gh

I. INTRODUCTION

Pattern formation associated with phase-transition kinetics is a problem of fundamental interest in statistical mechanics and finds important applications in materials science [1–5]. The typical phenomena studied in this context are formation of interconnected sponge-like structures via *spinodal decomposition* [4,6] of mixtures, dendritic crystal growth [7], spiral wave patterns in reaction-diffusion systems and biological systems [8,9], kinetics of mesophase formation in amphiphilic soft matter systems [10], and so on. Under many circumstances, the system is confined by external boundaries: The generic problem is phase-separation kinetics of binary mixtures (A,B) confined in thin films of thickness D (see Refs. [11–14] for recent reviews). The film surfaces provide boundary conditions for the Cahn-Hilliard-Cook (CHC) equation that describes the growth of A-rich and B-rich domains in the bulk of such a mixture. These boundary conditions cause the formation of a transient layered structure via a process termed as *surface-directed spinodal decomposition* (SDSD) [15]. An SDSD wave corresponds to a concentration profile with a wave vector oriented perpendicular to the wall and the wavelength $\lambda(t)$ growing with time t . The preparation of multicomponent thin films finds useful applications as protective coatings of surfaces, lubricants, templates for nanotechnology, etc., and, hence, many studies of SDSD can be found in the literature (e.g., experiments on polymer blend thin films are reviewed in Ref. [11]).

In the context of producing multicomponent thin films on substrates, it is rather natural to consider a situation where the concentration of the constituents across the film in the initial state is not constant but exhibits a gradient. For example, creating a thin film of a small-molecule mixture by vapor deposition, or by slow adsorption from a solution, it is possible that the composition of the vapor or solution changes gradually with time after the film growth has started. Further, external fields (gravity, electric fields, etc.) can also be responsible for thin films exhibiting such gradients. For example, anisotropic microporous polymer membranes

are produced via thermally induced phase separation of a polymer blend with an initial concentration gradient (the latter is produced by evaporating the diluent from the top surface of the film) [16]. Experimentally, one can also create composition gradients [17] by bringing a macroscopically segregated system back into the one-phase region, where the interface broadens by interdiffusion to any desired mesoscopic width and then quenching the system back into the miscibility gap. Thus, phase separation in a system with a concentration gradient arises in many contexts [17,18]. There have also been some preliminary theoretical studies of structure formation triggered by a region with a linear concentration gradient sandwiched between large regions of the bulk coexisting phases [18–21].

There has been intense interest [11–14] in the interplay of finite-size effects (associated with a nanoscopic film thickness) and preferential adsorption which may lead to layered structures in equilibrium [22,23]. However, the effects of composition gradients across a thin film and their interplay with the surface effects have so far received scant attention. It is the purpose of the present work to close this gap. We shall present model calculations to show that concentration gradients may stabilize very long-lived metastable morphologies, differing very much from the true equilibrium.

This paper is organized as follows. In Sec. II, we discuss our theoretical modeling. In Sec. III, we present detailed numerical results. Section IV concludes this paper with a summary.

II. THEORETICAL MODELING

The model that we study is the dimensionless version of the standard CHC equation with conserved order parameter Ψ (normalized to ± 1 in equilibrium) [1–5]:

$$\frac{\partial}{\partial t} \Psi(\vec{r}, t) = \vec{\nabla} \cdot \left\{ \vec{\nabla} \left[-\Psi + \Psi^3 - \frac{1}{2} \nabla^2 \Psi \right] + \vec{\theta}(\vec{r}, t) \right\}. \quad (1)$$

For studying thin films of thickness D , we restrict the z coordinate of the vector \vec{r} to the range $0 < z < D$. Note that,

for simplicity, we have assumed that the kinetic prefactors (describing the interdiffusion of particles, etc. [24]) are independent of Ψ . The units of time and length are chosen such that the mobility prefactor in Eq. (1) is absorbed in the time scale, and the prefactor of the $\nabla^2\Psi$ term is absorbed in the length scale, as is the standard practice [12–14]. The random noise $\bar{\theta}(\vec{r},t)$ satisfies the conditions (the overbar denotes a statistical average)

$$\overline{\theta_i(\vec{r},t)} = 0, \quad \overline{\theta_i(\vec{r}',t')\theta_j(\vec{r}'',t'')} = 2\epsilon\delta_{ij}\delta(\vec{r}' - \vec{r}'')\delta(t' - t''). \quad (2)$$

Here ϵ characterizes the strength of the noise. We use a finite linear dimension L with periodic boundary conditions in the x direction. In the z direction, which is perpendicular to the surfaces, we have a *no-flux* boundary condition at $z = 0, D$, i.e.,

$$\left\{ \frac{\partial}{\partial z} \left[-\Psi + \Psi^3 - \frac{1}{2}\nabla^2\Psi \right] + \theta_z \right\}_{z=0,D} = 0. \quad (3)$$

Additionally, we have boundary conditions describing the open surfaces [14]:

$$\frac{\partial}{\partial z}\Psi(x,z,t) \Big|_{z=0,D} = 0. \quad (4)$$

Note that the two surfaces are perfectly neutral (unlike Ref. [14], no surface field acts on Ψ).

The noise amplitude is chosen as $\epsilon = 0.041$, which corresponds to a deep quench with $T = 0.22T_c$, where T_c is the critical temperature of the bulk mixture [14]. Equations (1)–(4) are solved numerically via a Euler-discretization scheme with mesh sizes $\Delta z = \Delta x = 1$ and $\Delta t = 0.03$. Equations (4) are realized by setting $\Psi(x,0,t) = \Psi(x,1,t)$ and $\Psi(x,D+1,t) = \Psi(x,D,t)$.

The initial condition for a run consists of small-amplitude random fluctuations about a concentration gradient,

$$\Psi_{\text{av}}(z,t=0) \equiv \Psi_{\text{in}}(z) = (2z/D - 1)\Psi_g, \quad (5)$$

where Ψ_g characterizes the strength of the gradient. All statistical quantities presented here are obtained as averages over $n = 100$ independent runs (with different initial conditions). We have checked that our results are qualitatively unchanged for other choices of ϵ and/or smaller mesh sizes.

III. DETAILED RESULTS

There is broad evidence that (in the absence of concentration gradients) the phase-separation kinetics of systems in two dimensions ($L \times D$ geometry) and in three dimensions ($L \times L \times D$ geometry) is very similar [12–14]. Thus, we expect that it suffices to consider the simpler case of $L \times D$ systems (which needs much less computer time) even if we wish to address real systems in $d = 3$ dimensions. Figure 1 shows a series of evolution snapshots up to large times for $D = 50, L = 512$, and $\Psi_g = 0.2, 0.6$. At the shortest time shown ($t = 180$), the typical linear dimension $\ell(t)$ of the domains is much larger than unity but still clearly less than D . Thus, one has an irregular domain morphology, with relatively weak dependence on Ψ_g . For $t = 18000$, the domain size $\ell(t)$ has become comparable to D , but the domain walls are

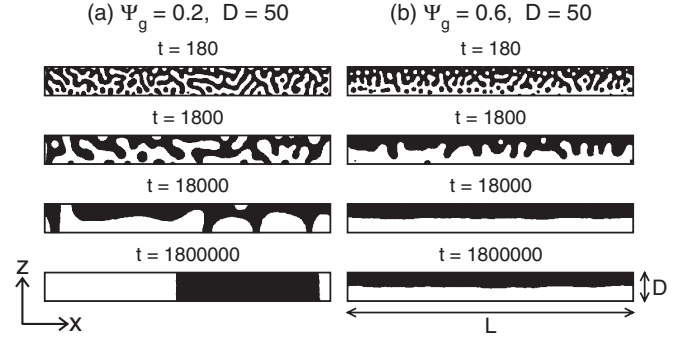


FIG. 1. Evolution snapshots of $D \times L$ thin films with $D = 50, L = 512$, for four times ($t = 180, 1800, 18000$ and 180000 , respectively). We show results for $\Psi_g = 0.2$ (a) and $\Psi_g = 0.6$ (b). Regions with $\Psi(x,z,t) > 0$ are shown in black, and regions with $\Psi(x,z,t) < 0$ are shown in white. We notice that the last snapshot in (a) exhibits two AB interfaces of length D , whereas the final snapshot in (b) exhibits a single interface of length L .

predominantly oriented parallel to the walls (particularly for large Ψ_g). However, when domain walls hit the surfaces, the contact angle is 90° , as expected for local equilibrium when no surface field acts (sphere-cap shaped droplets attached to the wall should then be semicircular). For the latest time shown in Fig. 1 ($t = 180000$), only the system with $\Psi_g = 0.2$ has reached the real equilibrium, i.e., two domains with walls perpendicular to the boundaries. This state has a total interfacial free-energy cost of $2\sigma D$, where σ is the AB surface tension. This is much less than the cost σL for the metastable layered structure [Fig. 1(b)] that persists for large Ψ_g . The layered structure can be destabilized by either of two mechanisms: (a) the long-wavelength sinusoidal deformation of the interface which hits the boundary of the film and (b) the nucleation and growth of a plug across the width of the film. Empirically, we find that the layered structure persists on the time scales of our simulation for $D = 50$ if $\Psi_g \geq 0.44$. We will shortly present arguments for the dependence of the critical value of Ψ_g on D .

We also note that crossing the mean-field spinodal at the boundaries ($\Psi_g > \Psi_{\text{sp}} \simeq 0.577$) does not lead to any significant differences in the growth behavior, as expected from experiment [17] and from general theoretical considerations [6]. The singular behavior at the spinodal results from a mean-field approach and is rounded off by fluctuations which we include in Eq. (1).

It may be argued that the situation considered in the present paper, namely a film with perfectly neutral walls (enforcing domain walls in equilibrium that are strictly perpendicular to the walls), is very special. However, we stress that the situation can readily be generalized to films confined by symmetric walls which prefer one of the phases. If we have equal amounts of both phases present in the film, we always have a final equilibrium state with one or two domain walls running across the film for $L \gg D$. (There are two domain walls if we apply periodic boundary conditions in the x direction and a single domain wall if free boundary conditions are used.) Of course, these domain walls are not straight but curved, depending on the boundary conditions acting at the walls.

Consider the limit where D is much larger than the intrinsic width of interfaces between coexisting phases, which, for the sake of illustration, we now call “vapor” (v) and “liquid” (l). The vapor-liquid interface then hits the “wall” (w) at a contact angle θ which obeys the well-known Young equation,

$$\gamma_{wv} - \gamma_{wl} = \gamma_{vl} \cos \theta. \quad (6)$$

Here γ_{wv} , γ_{wl} , and γ_{vl} denote the wall-vapor, wall-liquid, and vapor-liquid interfacial tensions. Since $|\cos \theta| \leq 1$, we have “complete wetting” if $\gamma_{wv} - \gamma_{wl} > \gamma_{vl}$ and “complete drying” if $\gamma_{wv} - \gamma_{wl} < -\gamma_{vl}$. In the first case, the wall will be coated by a (thin) wetting layer, so the actual interfacial energy of the vapor against the wall is $\gamma_{wv} = \gamma_{wl} + \gamma_{vl}$. In the second case, the wall is coated by a (thin) drying layer, so the actual liquid-wall free energy is $\gamma_{wl} = \gamma_{wv} + \gamma_{vl}$. The term *thin* refers to a layer whose thickness is negligible in comparison with the film thickness D but large in comparison with molecular distances (the thickness of such wetting/drying layers scales as $\ln D$ for short-range forces at the walls).

Figure 2 shows the structure of the system in the vicinity of the wall in the various regions that are of interest here. (Note that the “neutral wall” situation, corresponding to $\cos \theta = 0$, is just intermediate between “incomplete drying” and “incomplete wetting.”) In the region of incomplete drying and incomplete wetting, about half of the total boundary (the total boundary has the length $2L$) is exposed to the vapor and half to the liquid. Hence, the total interfacial energy due to the walls is $(\gamma_{wv} + \gamma_{wl})L$, since the contribution due to the vapor-liquid interface can be neglected for $D \ll L$. In this spirit, one also does not need to worry about contributions to the interfacial energy due to the three-phase contacts where the vapor-liquid interface hits the walls (Fig. 2, central part), nor about the curvature contribution to the vapor-liquid free energy, and so on. Uniformly layered structures (without interfaces running in the z direction across the strip) always cost more interfacial free energy than the equilibrium structures shown in Fig. 2(b). This argument remains true for other volume fractions $\phi, 1 - \phi$ of the two coexisting phases. A different situation could arise only in a system with “antisymmetric” walls, such that the lower wall favors the liquid and the upper wall favors the vapor, for example. In the case of complete wetting, one then has a single vapor-liquid interface running parallel to the walls. In the case of incomplete wetting, the interface runs across the strip from the lower wall to the upper wall, but it is not perpendicular to the walls; it is inclined according to the contact angle.

However, antisymmetric walls are hardly realized in practice, while symmetric walls (as considered in Fig. 2) are the generic case. Thus, the neutral wall case is a representative example of the behavior to be expected in practice. Moreover, if D is not much larger than the molecular scale, the wetting/drying transitions are strongly rounded and the change of the behavior encountered when one increases $\gamma_{wv} - \gamma_{wl}$ is rather gradual. On the molecular scale, neither the liquid nor the vapor phase is homogeneous near the walls, and, hence, these regions are not really distinct from wetting or drying layers which have only a thickness of a few molecular diameters. From the above discussion, it should be clear that including surface fields in the boundary condition in Eq. (4) adds interesting details (see Fig. 2) but will not modify the basic features of our description.

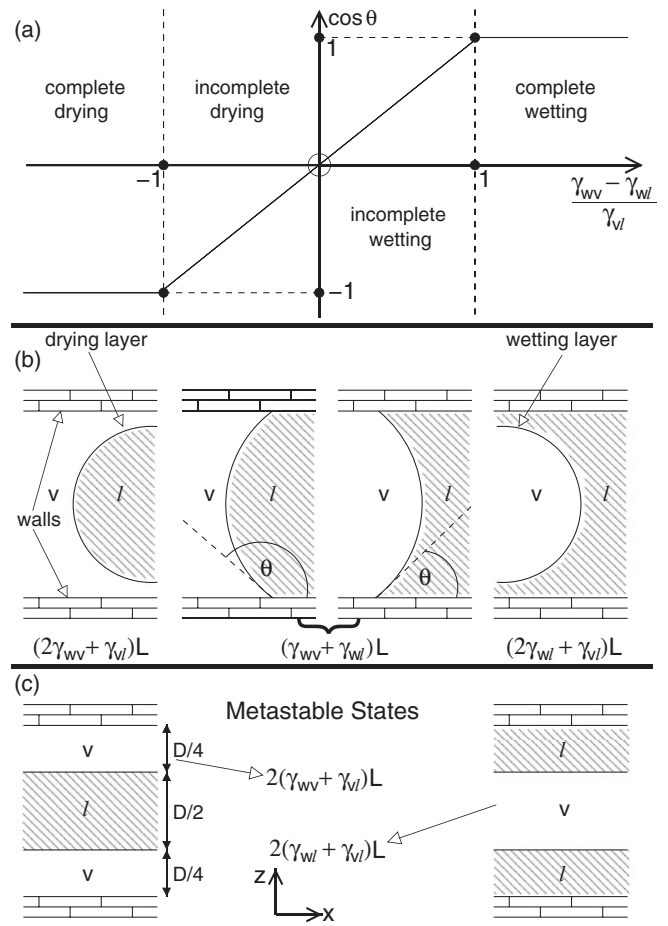


FIG. 2. (a) Graphical illustration of Young’s equation, showing $\cos \theta$ as a function of $(\gamma_{wv} - \gamma_{wl})/\gamma_{vl}$, indicating the regimes of complete and incomplete drying, as well as incomplete and complete wetting, respectively. (b) The equilibrium state [for the case where both coexisting phases, vapor (v) and liquid (l), occupy a volume fraction of 50% of the strip] contains an interface between the coexisting phases. On average, this runs perpendicular to the walls (w) at $x \simeq L/2$, irrespective of whether wetting/drying is complete or incomplete. For $(\gamma_{wv} - \gamma_{wl})/\gamma_{vl} < -1$ (complete drying), wall-liquid contact is avoided because of a thin drying layer, which leads to a cost of $2\gamma_{vl}(L/2)$ of vapor-liquid interfacial free energy, in addition to the free energy cost of the vapor at the two walls, $2\gamma_{wl}L$. Thus, the total free energy cost is $(2\gamma_{wv} + \gamma_{vl})L$. (c) However, if one considers a layered structure [left panel in (c)], the two vapor-liquid interfaces extend over L instead of $L/2$ only. Hence, the total free energy cost is $2(\gamma_{wv} + \gamma_{vl})L$. Likewise, the layered structure occurring under conditions of complete wetting [right frame of (c)] has an interfacial free energy cost $2(\gamma_{wl} + \gamma_{vl})L$. This exceeds the free energy cost of the equilibrium structure in (b), which is $(2\gamma_{wl} + \gamma_{vl})L$. In comparison with $\gamma_{vl}L$, the cost of the perpendicular interface ($\sim \gamma_{vl}D$) is always neglected, since $L \gg D$.

After this digression on the equilibrium state the system evolves toward, we now turn to the time evolution predicted by our model. Particularly interesting is the behavior of the order parameter profile $\Psi_{av}(z, t)$, averaged in the x direction parallel to the surfaces (Fig. 3). The initial linear profile [Eq. (5)] persists for some time in the central part of the film, while near the boundaries the linear profile is modulated

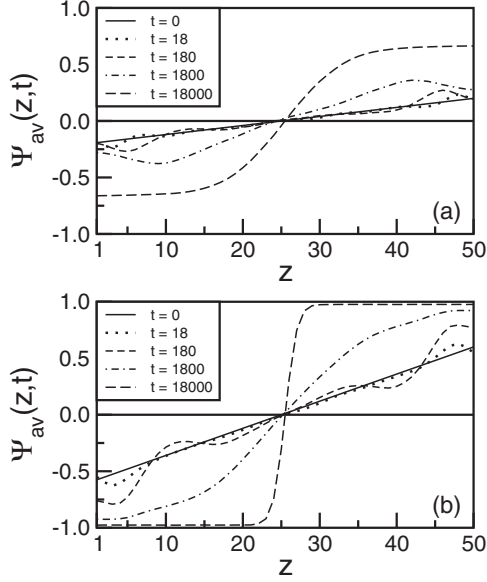


FIG. 3. Order parameter profiles, $\Psi_{av}(z,t)$ vs. z , averaged over the x direction parallel to the boundaries. We show results for $D = 50, L = 512$, and $\Psi_g = 0.2$ (a), $\Psi_g = 0.6$ (b). Five times t are shown, as indicated.

in a wavelike fashion, reminiscent of SDSD [11–14]. For thinner films with $D = 30$ (not shown), the waves starting from $z = 0$ and $z = D$ have already interfered near $z = D/2$ by $t = 180$. However, this is not the case for $D = 50$, where opposite SDSD waves coalesce for $t \simeq 1800$. When this interference has occurred, the extrema of $\Psi_{av}(z,t)$ at $z = 0, D$ start to become more pronounced. Further, $\Psi_{av}(z,t)$ resembles a sigmoidal profile like $\tanh[(z - D/2)/w(t)]$, with $w(t)$ being an effective time-dependent interfacial width.

Note that all the data sets shown in Fig. 3 only reflect the approach toward the layered metastable state with a single interface parallel to the walls, but not its decay. This decay is seen on the time scales of Fig. 3 ($t < 18000$) if we study thinner films, such as $D = 20$, and weaker gradients. In contrast, the same gradient for a much thicker film ($D = 70$) requires much longer to reach the metastable state with a single interface. The monitoring of its subsequent decay would require an enormous computing effort. The time scale for reaching the metastable state can be roughly estimated from a comparison of the length scale $R_1(t)$ (thickness of the enrichment layer of the SDSD wave) with $D/2$. The SDSD waves interact when $R_1(t) \sim D/2$. If $R_1(t) \ll D/2$, we still have the interconnected structure seen for $\Psi_g = 0.2, D = 50$, and $t = 180$. For $t = 1800$, one can already recognize a (very rugged) interface running on average in the x direction, while some bubbles (or droplets) are still present in both phases. At $t = 18000$, most bubbles and droplets have gone, and the interface has straightened out. Thus, the memory of the initial state with the gradient biases the structure of the system for very large times. We also emphasize that the lateral linear dimension L has been varied over a wide range ($256 \leq L \leq 2048$) but the results are independent of L .

If one estimates that $R_1(t)$ grows like the bulk length scale for a system with conserved order parameter [25], $\ell_b(t) \sim t^{1/3}$, the condition $R_1(t) \sim D/2$ yields $t_{ms} \sim D^3$ (neglecting

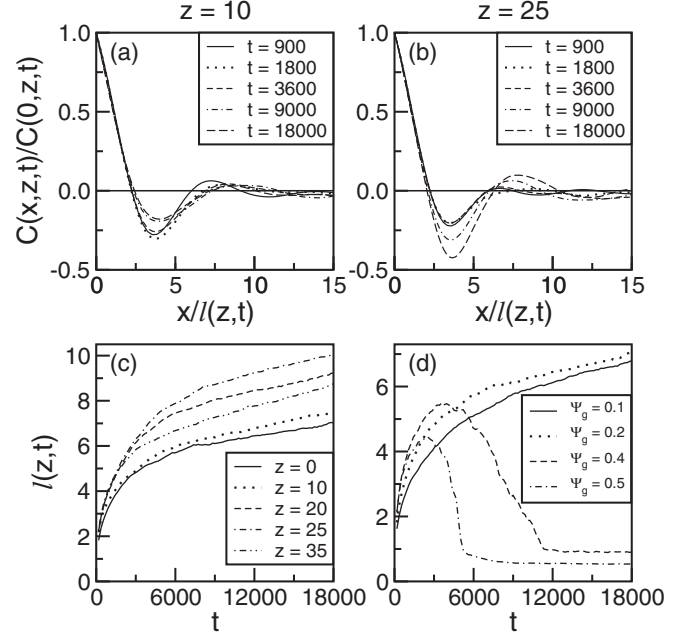


FIG. 4. Normalized correlation functions $C(x,z,t)/C(0,z,t)$ vs. $x/l(z,t)$ for $\Psi_g = 0.2$ and $z = 10$ (a), and $z = D/2 = 25$ (b). Panel (c) shows the time dependence of the length $\ell(z,t)$ for various layers, as indicated. Panel (d) shows $\ell(z = 0, t)$ for several values of Ψ_g .

all prefactors of order unity). However, the time to nucleate a perpendicular domain wall is much larger, $t_{\text{plug}} \sim \exp(\sigma D)$, since the interface tension σ in our model is of order unity. In order to quantify the evolution of the structure, we consider the layerwise correlation function (Fig. 4)

$$C(x,z,t) = L^{-1} \int_0^L dx' [\langle \Psi(x',z,t) \Psi(x' + x, z, t) \rangle - \langle \Psi(x',z,t) \rangle \langle \Psi(x' + x, z, t) \rangle], \quad (7)$$

or its Fourier transform $S(k,z,t)$. Both quantities can be used to introduce characteristic length scales, e.g., $\ell(z,t)$ can be defined from $C[x = \ell(z,t), z, t] = C(0, z, t)/2$. For bulk phase separation, one has the Lifshitz-Slyozov growth law, $\ell_b(t) \sim t^{1/3}$ (independent of z); and the correlation function $C(r,t)$ yields a universal scaling function $\tilde{C}(r/\ell_b)$ [1–5]. However, such a scaling does not work in the presence of a gradient [Figs. 4(a) and 4(b)]. Further, the layerwise length scale $\ell(z,t)$ shows a monotonic increase with t for small Ψ_g [Fig. 4(c)], but, near the boundaries, a nonmonotonic behavior prevails for large Ψ_g [Fig. 4(d)].

The similarity of the profile $\Psi_{av}(z,t)$ to SDSD can actually be put on a quantitative basis, as the following argument shows. We linearize Eq. (1) with $\bar{\theta} = 0$ about the initial state Ψ_{in} introduced in Eq. (5), $\Psi(\vec{r}, t) = \Psi_{in}(z) + \phi(\vec{r}, t)$. In the case of a small linear gradient ($\Psi_g \ll 1$), we obtain [$\Psi'_{in}(z) = d\Psi_{in}(z)/dz$]

$$\begin{aligned} \frac{\partial}{\partial t} \phi(\vec{r}, t) &= \nabla^2 \left[-\phi - \frac{1}{2} \nabla^2 \phi - \Psi_{in}(z) \phi - \frac{1}{2} \Psi''_{in}(z) \phi^2 \right] \\ &= \nabla^2 \left(-\phi - \frac{1}{2} \nabla^2 \phi \right). \end{aligned} \quad (8)$$

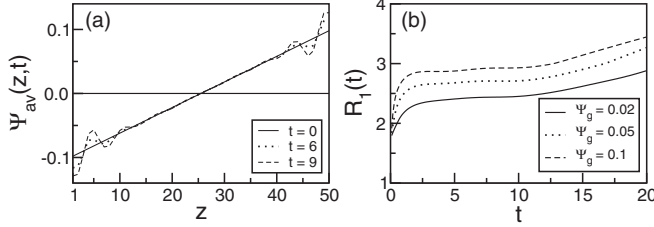


FIG. 5. Early-time results for the case with no noise ($\epsilon = 0$). (a) Laterally averaged profiles for $t = 6, 9$, reminiscent of SDSA waves. The parameters are $\Psi_g = 0.1$ and $D = 50$. (b) Plot of the first intersection of $\Psi_{av}(z, t)$ with $\Psi_{in}(z)$, $R_1(t)$ vs. t , for the profiles corresponding to $D = 50$ and $\Psi_g = 0.02, 0.05, 0.1$.

The corresponding boundary conditions are

$$\left. \frac{\partial \phi}{\partial z} \right|_{z=0} = \left. \frac{\partial \phi}{\partial z} \right|_{z=D} = -\Psi'_{in}(z) \Big|_{z=0,D} = -\frac{2\Psi_g}{D}. \quad (9)$$

In the case of SDSA with short-range surface forces, the same equation [Eq. (8)] results and the standard boundary conditions are [11–14]

$$\begin{aligned} h_1 + g\Psi + \gamma \left. \frac{\partial \Psi}{\partial z} \right|_{z=0} &= 0, \\ h_D + g\Psi - \gamma \left. \frac{\partial \Psi}{\partial z} \right|_{z=D} &= 0. \end{aligned} \quad (10)$$

Here, the constants h_1, h_D are the local surface fields (coupling linearly to the order parameter). The parameters g, γ depend on the change of pairwise interactions near the surface of the underlying microscopic model (e.g., a spin-exchange kinetic Ising model). Comparing Eqs. (9) and (10), we see that Eq. (9) is a special case of Eq. (10) with $g = 0$ and *antisymmetric* wall potentials, $h_1/\gamma = -h_D/\gamma = 2\Psi_g/D$ [22]. Thus, we expect that the initial stages of SDSA (where a concentration wave forms near the surface, with an enrichment layer at each surface oriented along the surface field, followed by a depletion layer) also arise in the present case. To test this consideration more quantitatively, Fig. 5(a) shows a counterpart of Fig. 3, where very early times ($t < 10$) are considered and we set $\epsilon = 0$ in Eq. (1) (so only the noise in the initial state is amplified). Indeed, one sees [Fig. 5(b)] that the first intersection of the growing waves near the boundary with $\Psi_{in}(z)$ (denoted as R_1) stays independent of time at early times. The wavelength is comparable with the theoretical value that follows from Eq. (8) for the waves with the maximum growth rate, $\lambda_m = 2\pi$ (note that this result is not precisely reproduced due to the coarseness

of the discretization, which was $\Delta z = 1/2$ in this case). At times $t > 10$, coarsening already sets in (the nonlinear term in Eq. (1) matters when the fluctuations of the initial state have been magnified enough on the scale of λ_m [4,6]).

Before concluding, let us clarify the conditions governing the formation of the layered state. In the absence of any concentration gradient, domains grow isotropically in the film according to the LS growth law, $\ell_b(t) \sim (\sigma t)^{1/3}$. Thus, the growing domains form a bridge across the film on a time scale $t_{br} \sim D^3/\sigma$. On the other hand, the SDSA profiles reach the center of the film and coalesce on a time scale t_{layer} given by the condition $R_1(t_{layer}) \sim D/2$. In the late stages of wetting-layer growth, we have $R_1(t) \sim h_1(\sigma t)^{1/3}$ [25], so $t_{layer} \sim D^3/(h_1^3\sigma)$. The layered state forms when $t_{layer} \ll t_{br}$ or $h_1 \gg 1$. Recalling that $h_1 = 2\Psi_g/D$, we expect that the critical value of Ψ_g for formation of the metastable layered state scales linearly with D . Given that $\Psi_g^c \simeq 0.44$ for $D = 50$, we can estimate $\Psi_g^c \simeq 0.0088D = D/D_m$ (with $D_m \simeq 113.63$) for arbitrary D values. The above arguments are valid for $D \ll D_m$. What about the case with $D \gg D_m$? In this case, the z dimension of the “film” is very large. The wetting layer does not grow to such macroscopic sizes as the growth of lateral fluctuations destroys the layered structure at large distances from the surfaces, i.e., we do not expect the formation of a layered metastable state for $D \gg D_m$.

IV. SUMMARY

In summary, we have shown that a small concentration gradient in an otherwise random initial state of a thin film of a mixture causes an extremely long-lived memory in the subsequent phase-separation process, leading to metastable layered structures for a broad range of conditions. For weak gradients, this process has strong similarities to *surface-directed spinodal decomposition* in thin films with antisymmetric boundary conditions. It would be interesting to explore the complications created if static (in general asymmetric) boundary conditions such as Eq. (10) exist in addition to gradients. We propose that initial gradients should be useful to produce various metastable domain patterns via phase separation processes.

ACKNOWLEDGMENTS

One of us (P.K.J.) is grateful to the Max Planck Institute for Polymer Research (MPIP) for support through a fellowship, and another (S.P.) thanks the Deutsche Forschungsgemeinschaft (SFB 625/A3) for travel support.

- [1] A. J. Bray, *Adv. Phys.* **43**, 357 (1994).
- [2] G. Kostorz (ed.), *Phase Transformations in Materials* (Wiley-VCH, Weinheim, 2001).
- [3] A. Onuki, *Phase Transition Dynamics* (Cambridge University Press, Cambridge, 2002).
- [4] S. Puri and V. K. Wadhawan (eds.), *Kinetics of Phase Transitions* (CRC Press, Boca Raton, FL, 2009).

- [5] R. C. Desai and R. Kapral, *Dynamics of Self-Organized and Self-Assembled Structures* (Cambridge University Press, Cambridge, 2009).
- [6] K. Binder and P. Fratzl, in *Phase Transformations in Materials* (Wiley-VCH, Weinheim, 2001), chap. 6.
- [7] H. Müller-Krumbhaar and W. Kurz, in *Phase Transformations in Materials* (Wiley-VCH, Weinheim, 2001), chap. 10.

- [8] S. Kim, K. J. Lee, and W. Sung (eds.), *Stochastic Dynamics and Pattern Formation in Biological and Complex Systems* (AIP, Melville, NY, 2000).
- [9] A. Goldbeter, *Biochemical Oscillations and Cellular Rhythms: The Molecular Basis of Periodic and Chaotic Behavior* (Cambridge University Press, Cambridge, 1996).
- [10] T. Ohta, in *Kinetics of Phase Transitions* (CRC Press, Boca Raton, FL, 2009), chap. 7.
- [11] M. Geoghegan and G. Krausch, *Prog. Polym. Sci.* **28**, 261 (2003).
- [12] S. Puri and H. L. Frisch, *J. Phys.: Condens. Matter* **9**, 2109 (1997); S. Puri, *ibid.* **17**, R101 (2005).
- [13] K. Binder, S. K. Das, and J. Horbach, *Mod. Phys. Lett. B* **23**, 549 (2009).
- [14] K. Binder, S. Puri, S. K. Das, and J. Horbach, *J. Stat. Phys.* **138**, 51 (2010).
- [15] R. A. L. Jones, L. J. Norton, E. J. Kramer, F. S. Bates, and P. Wiltzius, *Phys. Rev. Lett.* **66**, 1326 (1991).
- [16] H. Matsuyama, M. Yuasa, Y. Kitamura, M. Teramoto, and D. R. Lloyd, *J. Membr. Sci.* **179**, 91 (2000).
- [17] Y. Jayalakshmi, B. Khalil, and D. Beysens, *Phys. Rev. Lett.* **69**, 3088 (1992); D. Beysens and Y. Jayalakshmi, *Physica A* **213**, 71 (1995).
- [18] G. Santonicola, R. Mauri, and R. Shinnar, *Ind. Eng. Chem. Res.* **40**, 2004 (2001).
- [19] A. M. Lacasta, J. M. Sancho, and C. Yeung, *Europhys. Lett.* **27**, 291 (1994).
- [20] P. K. Chan, *Modelling Simul. Mater. Sci. Eng.* **14**, 41 (2006); S. Hong and P. K. Chan, *Modell. Simul. Mater. Sci. Eng.* **18**, 025013 (2010).
- [21] B. T. Jiang and P. K. Chan, *Macromol. Theory Simul.* **16**, 690 (2007).
- [22] S. K. Das, S. Puri, J. Horbach, and K. Binder, *Phys. Rev. E* **72**, 061603 (2005); **73**, 031604 (2006); *Phys. Rev. Lett.* **96**, 016107 (2006).
- [23] D. Bonn, J. Eggers, J. Indekeu, J. Meunier, and E. Rolley, *Rev. Mod. Phys.* **81**, 739 (2009).
- [24] S. Puri, A. J. Bray, and J. L. Lebowitz, *Phys. Rev. E* **56**, 758 (1997).
- [25] S. Puri and K. Binder, *Phys. Rev. Lett.* **86**, 1797 (2001); *Phys. Rev. E* **66**, 061602 (2002).